Passive source location by diffraction scanning

Jorge E. Monsegny[1], Don C. Lawton[1,2] and Daniel Trad[1]
[1]CREWES, University of Calgary; [2]Carbon Management Canada

ABSTRACT

During CO_2 injection monitoring several events generated by passive sources at different locations are recorded. Some events are from surface operations while others are consequence of the CO_2 injection. We use a technique that analyzes the moveout of the passive seismic events for a series of potential sources located at different positions in the subsurface. The technique generates a plot that catalogs the events by source location making possible to discern events produced the zone of interest from events generated elsewhere. We apply the technique to passive seismic records at the Containment and Monitoring Field Research Station in Alberta, Canada.

INTRODUCTION

CO_2 injection can cause fracturing (Yew and Weng, 2015) and this fracturing can manifest itself in passive seismic records. For this reason it is important to monitor the seismic activity in a CO_2 injection facility and look for microseismic events generated in the injection zone.

Nagano et al. (1989) analyze a triaxial hodogram to locate sources and measure subsurface cracks. This technique requires the extraction of P and S waves arrivals. Rost and Thomas (2002) review different seismic arrays techniques used in seismology to localize events. Gajewski et al. (2007) use the diffraction stack of the squared amplitudes in a seismogram to localize seismic events. Lu et al. (2014) automatically identify the apexes of seismic events in shallow water surveys and their positions are used to calculate the source locations. Khoshnavaz et al. (2017) use the local slopes of the seismic events moveout to locate the source position. An advantage of this technique is that it does not require a detailed velocity model. Liu et al. (2020) propose interferometric and autocorrelation methods to locate passive seismic sources by the seismic energy emitted during hydraulic fracturing.

CaMI-FRS stands for Containment and Monitoring Institute Field Research Station. It is a research facility located near Brooks in Alberta, Canada where small volumes of CO_2 are being injected yearly at a depth close to 300m (Macquet et al., 2019). To monitor the reservoir state during the injection a set of technologies are deployed there like multicomponent geophone arrays, distributed acoustic sensing (DAS) and electrical resistivity arrays, both at the surface and inside two observation wells located close to the injection well (Lawton et al., 2017).

In this report we use a technique that analyzes the moveout from several potential seismic sources and catalogs the events in a passive seismic record by the probable source depth. In this way we are able to distinguish seismic events generated at the surface from the ones generated in the CO_2 injection zone.

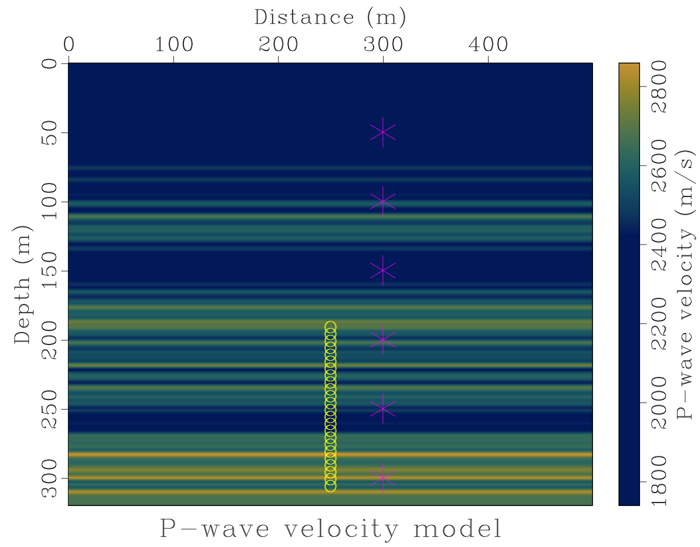

FIG. 1. Velocity model at CaMI-FRS obtained from well data. Superimposed are the geophone locations inside the well (circles) and six passive sources (asterisks) used to illustrate the moveout analysis.

First we are going to show the moveout analysis technique concept with a synthetic experiment. Then we are going to use the technique in a series of passive records from CaMI-FRS where the events from surface operations can be separated from potential events from the CO_2 injection zone.

METHODS

We are going to illustrate the moveout analysis method using a synthetic example. This example will show the principal aspects of the technique.

Figure 1 shows the velocity model at CaMI-FRS obtained from well data. The circles below the lateral position 250m and from 191m to 306m deep each 5m are the locations of the receiver array inside the observation well. The asterisks below the 300m lateral position are the locations of six passive sources that are going to be used to illustrate the moveout analysis. Their vertical coordinates go from 50m deep to 300m deep every 50m.

The first arrivals or moveout from each of these sources with respect to the receiver array inside the well is different. In principle any method to calculate these traveltimes can be used, subject to the desired accuracy and the computational expense. In this case we used fast marching (Sethian and Popovici, 1999) because we can store the traveltimes from every subsurface position and use them again when more sources are scanned or when more receivers are added to the array.

Figure 2 shows the moveout curves from the sources to the receiver array in Figure 1. In the figure each curve is labelled with its corresponding source depth. The moveout of sources at 50m, 100m and 150m depth show a linear trend while the corresponding moveout of sources at 200m, 250m and 300m is more curved. This is mainly due to the aperture of the array, but is also a pattern that the moveout scan can take advantage of.

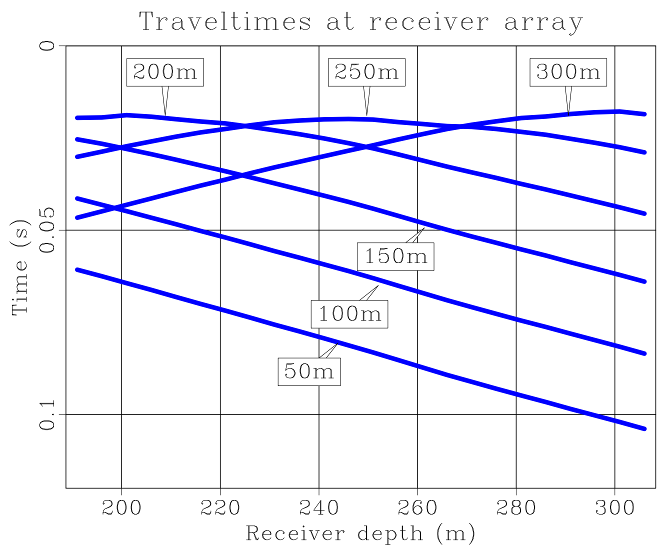

FIG. 2. Traveltimes of moveout curves from the sources to the receiver array in Figure 1. Each curve is labelled with the depth of its corresponding source.

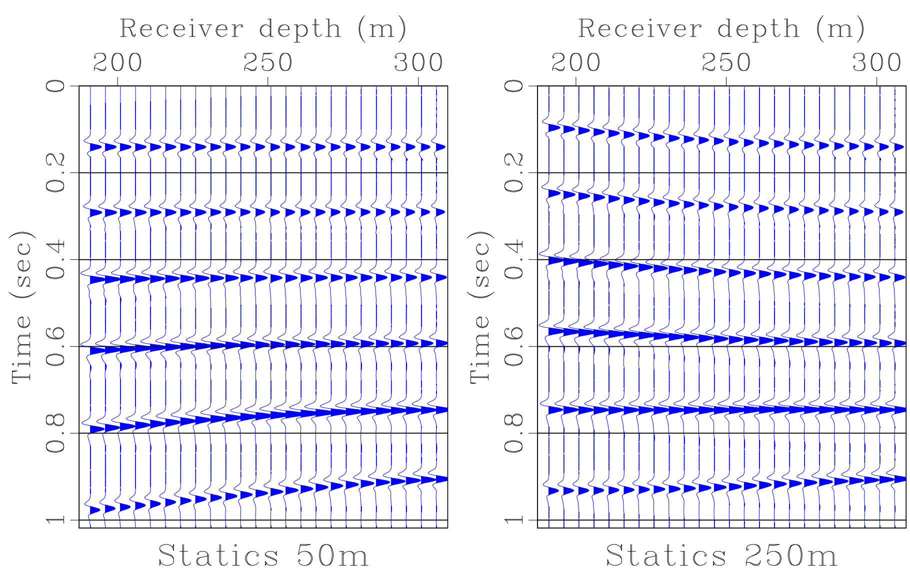

FIG. 3. The traveltimes curves are applied like static corrections to the shot gather. On the left is the corrected gather with the 50m deep source and on the right is the one with the 250m deep source.

In the left part of Figure 5 is the synthetic shot gather. Each event corresponds to one of the six sources in Figure 1. Each source was activated in sequence from top to bottom, with a small time between them to avoid that the events cross each other. The shape of each event follows the moveout of the corresponding traveltime curve in Figure 2.

Each traveltime curve is used as a static correction and is applied to the shot gather. For example, Figure 3 shows the static corrected gathers by traveltime curves from sources at $50\mathrm{m}$ and $250\mathrm{m}$ deep.

In order to be able to reference events from the shot gather before and after the static correction is applied, the moveout curves are modified in the following way. At the deepest geophone the correction is set to null while the other values are set relative to it. In this way the deepest trace is always the same before and after applying the static corrections.

Something to notice after applying the static corrections in Figure 3 is that the events that correspond to the moveout curve align horizontally while the others have some angle with respect to the horizontal. This horizontal alignment increases the lateral similarity of the traces. We use the semblance to measure this similarity. The semblance S_T at time t is defined as:

$$S_T(t) \stackrel{\text{def}}{=} \frac{\sum_{\tau=t-m\Delta}^{t+m\Delta} \left(\sum_{i=1}^{N} g_{\tau,i} \right)^2}{N \sum_{\tau=t-m\Delta}^{t+m\Delta} \sum_{i=1}^{N} (g_{\tau,i})^2}, \tag{1}$$

where $m\Delta$ defines a small time window around t, N is the number of traces and $g_{\tau,i}$ is the sample at trace i and time τ (Sheriff, 2002). Semblance values are between 0 and 1 and it can be proved that they are 1 when the traces are equal (Geldart and Sheriff, 2004).

It is usual that the source position is unknown. For that motive we generate moveout curves for a set of sources in an area around the receiver array. In this synthetic example we use sources from $0\mathrm{m}$ to $250\mathrm{m}$ every $10\mathrm{m}$ in the lateral direction and from $0\mathrm{m}$ to $320\mathrm{m}$ every $10\mathrm{m}$ in the vertical direction. Figure 4 displays the sources positions. All the moveout curves are referenced to the deepest trace, applied as static corrections and the semblance of the corrected gather is calculated as explained before.

The right part of Figure 5 shows the moveout scan plot of the synthetic gather. This plot is composed of a series of depth stripes and inside each stripe there are semblances for different horizontal positions. It can be argued that a 3D plot is more appropriate but we are going to continue showing this plot in 2D.

Due that the static corrections were referenced with respect to the deepest trace it is possible to follow horizontally each event on the shot gather to its corresponding semblance value on the moveout scan plot. The events from sources at $50\mathrm{m}$ to $200\mathrm{m}$ deep have high

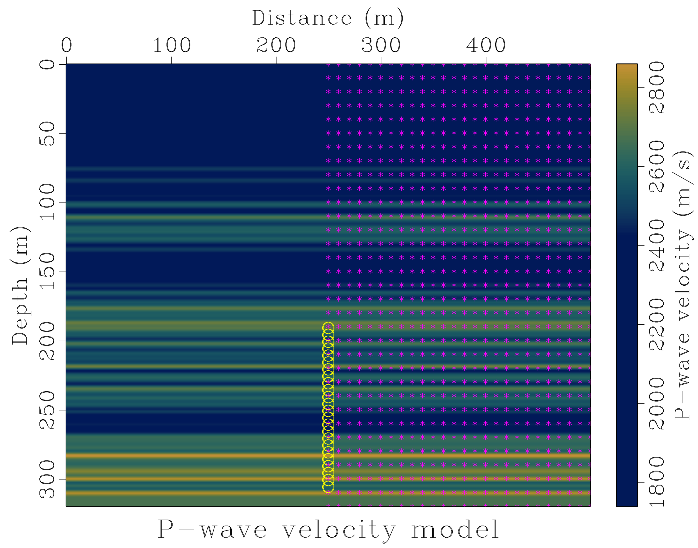

FIG. 4. Velocity model at CaMI-FRS obtained from well data. Superimposed are the geophone locations inside the well (circles) and passive sources (asterisks) used in the synthetic and field data examples.

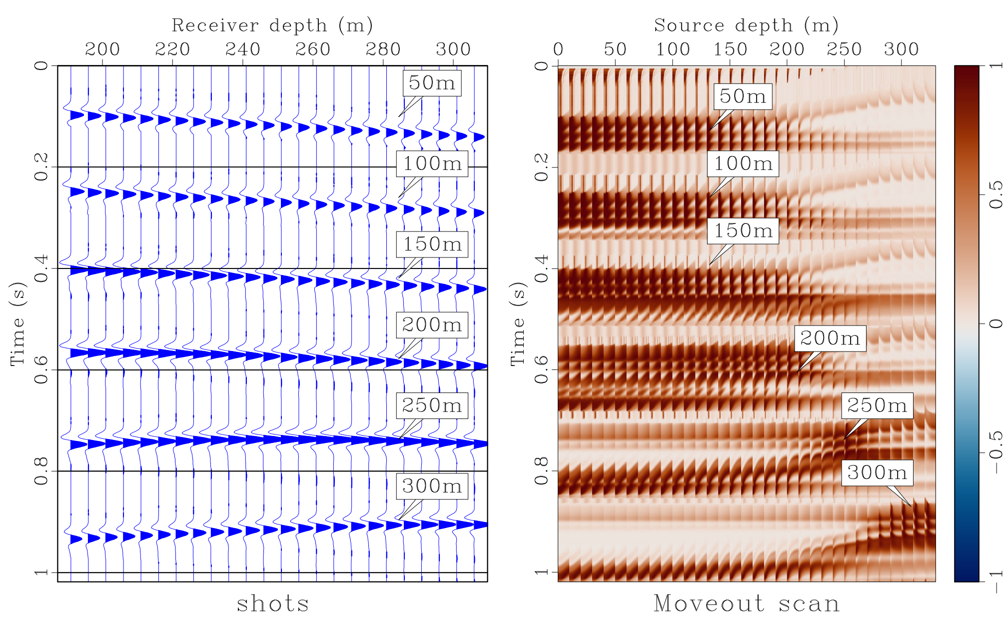

FIG. 5. On the left is the synthetic shot gather with the first arrival events from each of the sources in Figure 1. Each event is labelled with the source depth. They do not overlap because the sources were activated in sequence with a time delay between them. On the right is the moveout scan plot of the synthetic shot gather with labels showing the semblance highest value zone of each event.

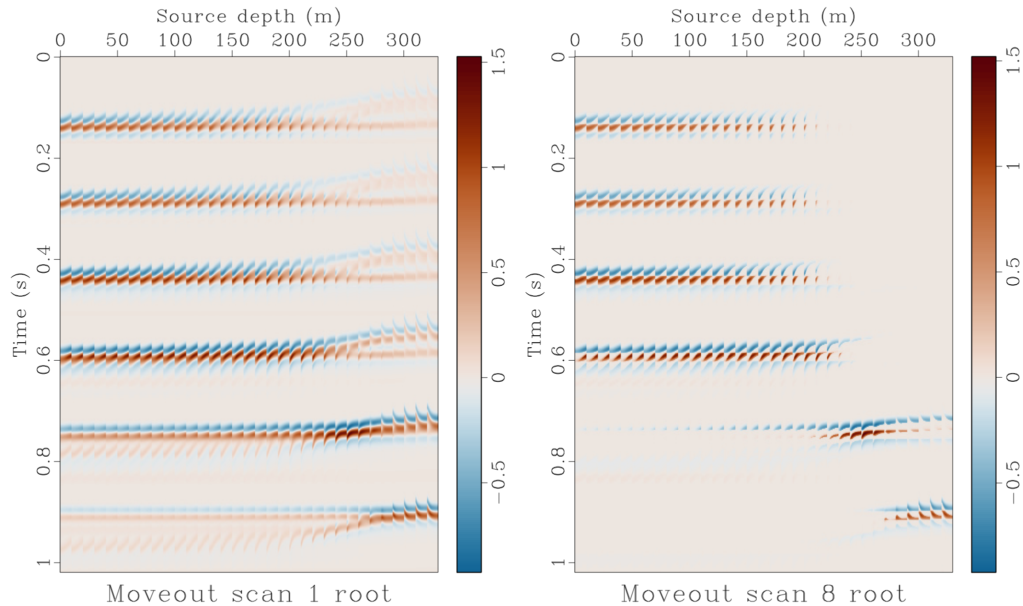

FIG. 6. On the left is the 1st root stack or simple stacking of the gather in Figure 5. On the right is the 8-th root stack.

semblance values for sources between 0m and 200m. In contrast, the events from sources at 250m and 300m deep have more localized semblance values around their true source depths.

Kanasewich et al. (1973) proposed the n-th root stack method to enhance the events while reducing random noise. This method stacks the signed n-th root data amplitude first:

$$r'_n(t) = \frac{1}{N}\sum_{i=1}^{N} |g_{t,i}|^{1/n} sign(g_{t,i}) \tag{2}$$

and then restores the signed amplitudes after stacking:

$$r_n(t) = |r'_n(t)|^n sign(r'_n(t)) \tag{3}$$

with the same notation as before. Figure 6 displays the results of this technique. On the left is the 1st root or simple stack and on the right is the 8-th root stack. This technique shows better the position of the sources but at the expense of the low energy events.

The effect of noise in the data is shown in Figure 7. In the left we added zero mean normal noise with variance equal to one third to the synthetic gather. In the center and right are the semblance moveout scan and the 8-th root stack. It seems that the presence of noise improves both moveout scan plots.

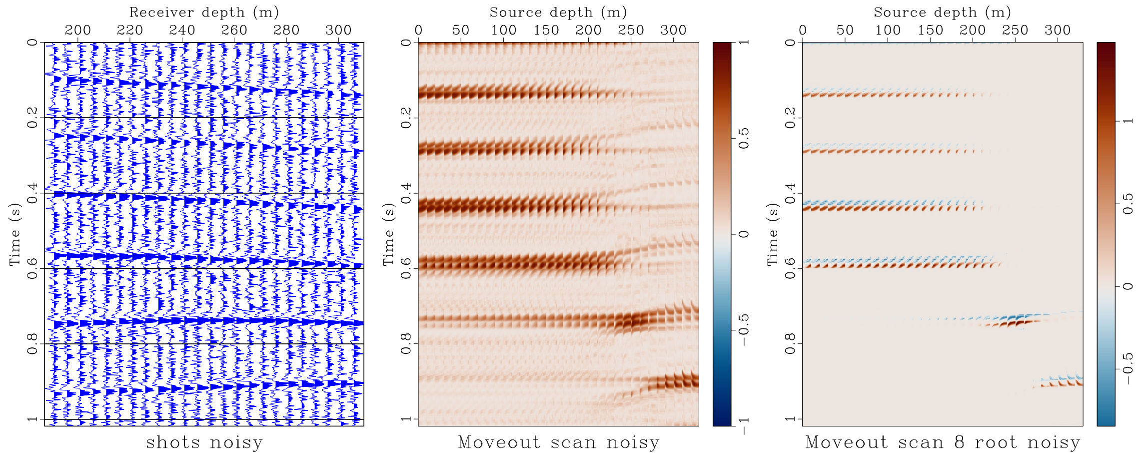

FIG. 7. Moveout scan with noise. Left is the synthetic shot gather plus zero mean normal noise with variance equal to one third. Center and right show the semblance moveout scan and the 8-th root stack, respectively.

FIELD DATA

We used data from CaMI-FRS to test the moveout scan technique. The velocity model and receiver array are the same of Figure 1. We also scanned the same set of sources than in the synthetic example and that means that we used again the precomputed moveout curves.

The CaMI-FRS observation well receiver array is composed of multicomponent geophones and we analyze the vertical component because it is the most energetic. Due that the potential sources have different depths with respect to the array, a polarity change is expected in this component. This polarity change is akin to the one observed in active surface seismics in the inline component.

To address this complication, during each semblance calculation we reversed the polarity of the seismic gather below the source depth. This works when the velocity model is simple but when not, an approach that detects the moveout local maxima and minima and reverse the traces between them can be implemented.

The left part of figures 8 and 9 show a portion of a passive seismic record. The only preprocessing was the deletion of some very noisy traces and the application of a $5-50$Hz filtering to suppress high frequency noise.

Several events are evident in the seismic record and by following them horizontally to the moveout plot on the right part of the same figures it can be seen that their probable sources are located in a broad area above 200m.

In contrast, some parts of the moveout plot shows probable events below 200m. Events labelled A and B have potential sources below 300m while the ones labelled C and D have sources between 250m and 300m. Although their semblance values are high the actual seismic events in the gather are faint.

Figures 10 and 11 are another example, showing a 15 minutes seismic record. During

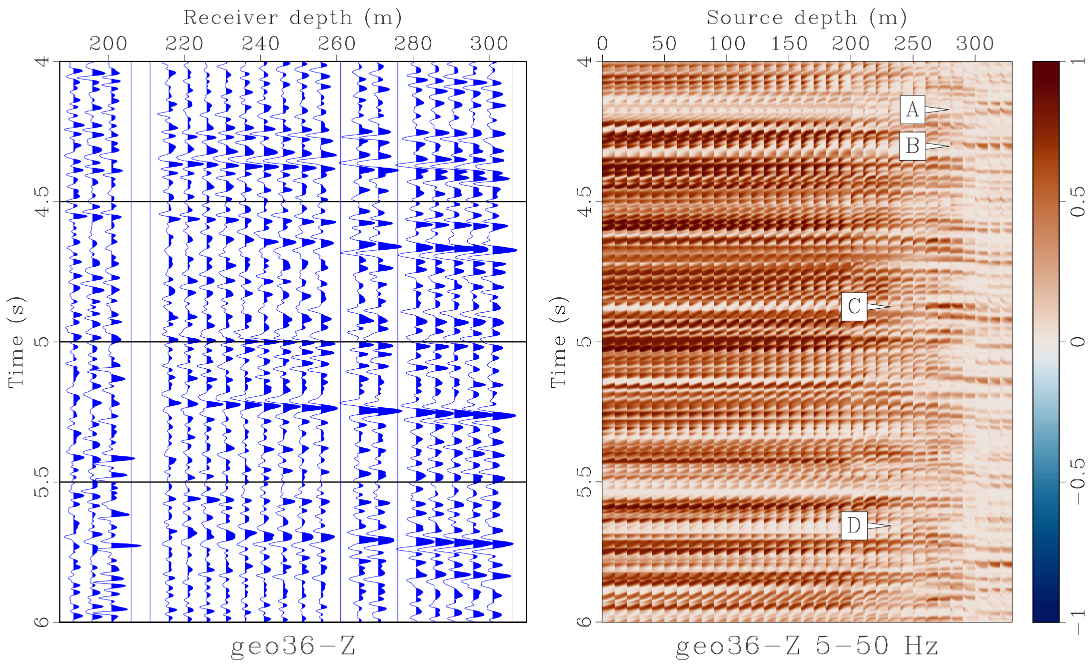

FIG. 8. Passive seismic record and moveout semblance plot. The most important features in the record have high semblance values above $200m$. Other features, labelled A through D have high semblance values below $200m$.

that time a trailer on the surface was skidding and steering. This record had the same processing than the previous one. The moveout plots show that the more prominent events are from sources above 200m. On the other hand, there are silence periods when the plot shows high values in the zone below 200m. Similar to the previous example, the corresponding events are faint in the seismic record.

DISCUSSION

The moveout plots can distinguish events generated below and above 200m deep. This is due to the aperture of the receiver array. In the future we plan to use DAS data that spans all the well to increase the moveout resolving power.

Several artifacts appear in the moveout plots in Figure 5. They are due to the sidelobes and the semblance normalization effect. A careful interpretation of this plot is needed.

The Radon Transform (Durrani and Bisset, 1984) can detect linear and parabolic events in seismic records. However it does not manage general velocity models like the moveout plot and does not convey the source locations.

For events generated above 200m the semblance plot gives a very wide source location. This can also be fixed by increasing the receiver array aperture.

ACKNOWLEDGEMENTS

We thank the sponsors of CREWES for continued support. This work was funded by CREWES industrial sponsors and NSERC (Natural Science and Engineering Research

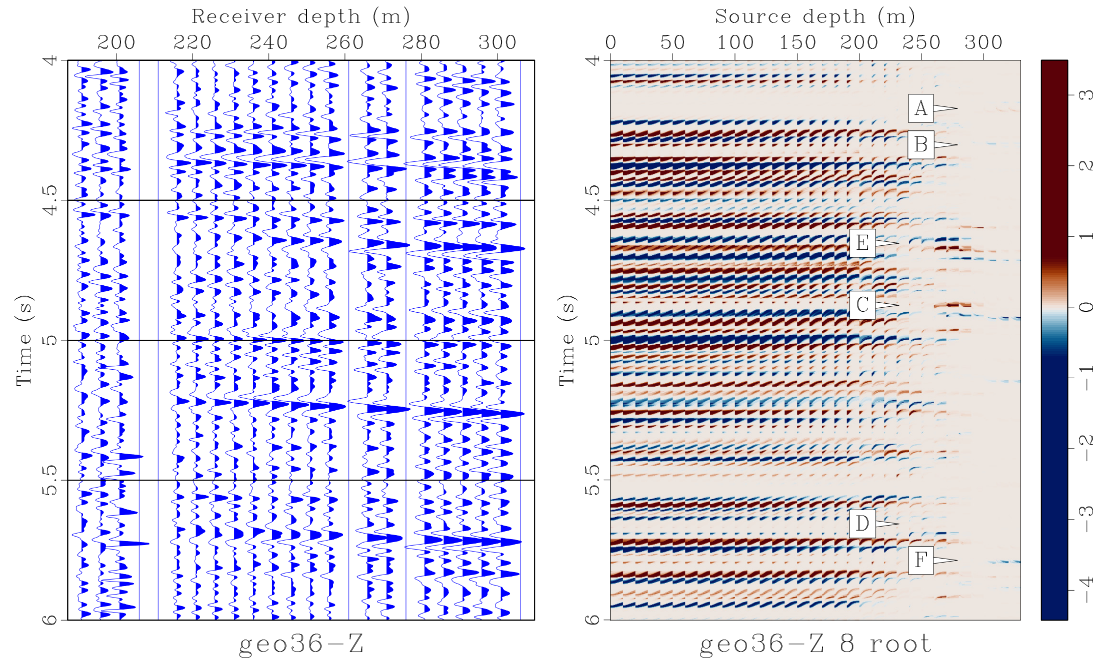

FIG. 9. Passive seismic record and moveout 8-th root stacking plot. The most important features in the record have high semblance values above $200m$. Other features, labelled A through D have high semblance values below $200m$. Feature labelled F is another possible event.

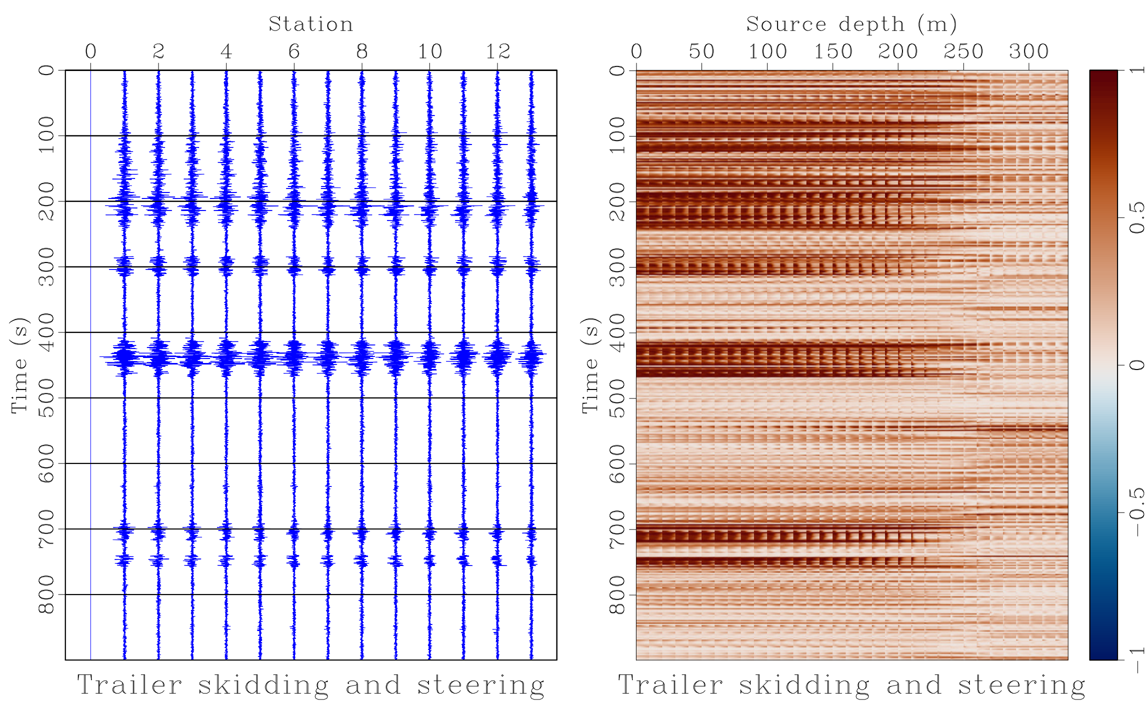

FIG. 10. Fifteen minutes passive seismic record while a trailer was skidding and steering on the surface. The semblance plot is on the right. Most of the events come from sources located above $200m$, however there are events with sources below this depth, especially during quiet times.

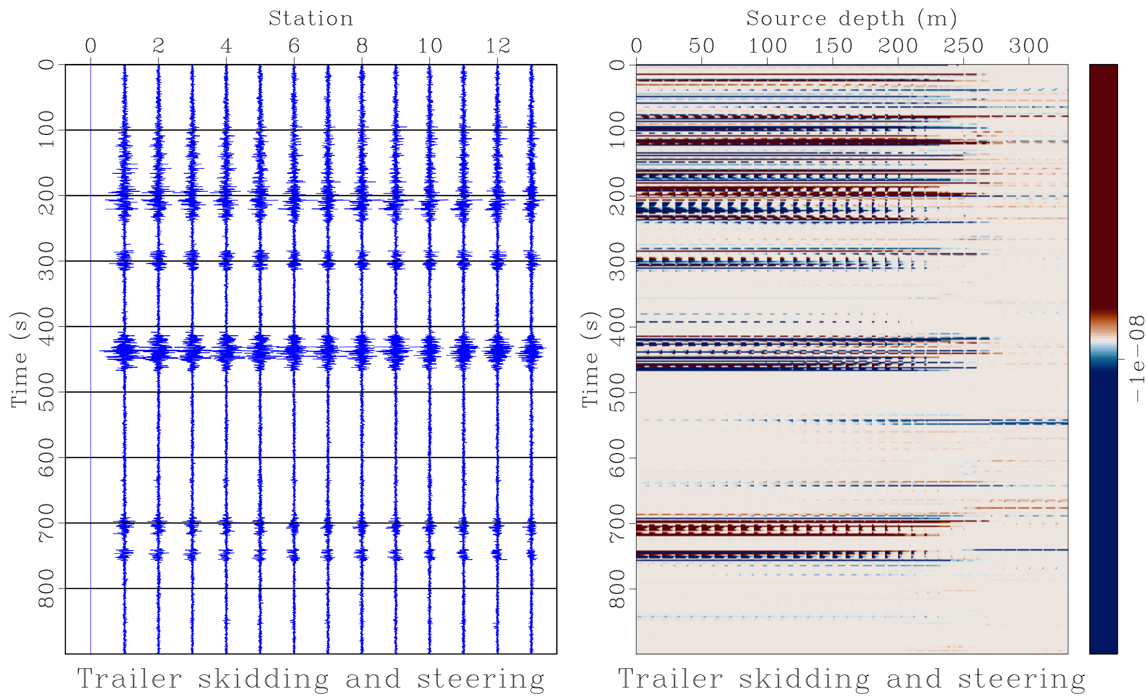

FIG. 11. Fifteen minutes passive seismic record while a trailer was skidding and steering on the surface. The 8-th root stacking plot is on the right. As before, most of the events come from sources located above $200m$, however there are events with sources below this depth, especially during quiet times.

Council of Canada) through the grant CRDPJ 543578-19. The data were acquired through a collaboration with Containment and Monitoring Institute (CaMI) of Carbon Management Canada (CMC). Research at the CaMI field site is supported in part by the Canada First Research Excellence Fund, through the Global Research Initiative at the University of Calgary and the CaMI.FRS Joint Industry Project. The first author (JM) is also supported by Canada First Research Excellence Fund, through the Global Research Initiative at the University of Calgary

REFERENCES

Durrani, T. S., and D. Bisset, 1984, The radon transform and its properties: GEOPHYSICS, **49**, 1180–1187.

Gajewski, D., D. Anikiev, B. Kashtan, E. Tessmer, and C. Vanelle, 2007, Localization of seismic events by diffraction stacking: SEG Technical Program Expanded Abstracts 2007, 1287–1291.

Geldart, L. P., and R. E. Sheriff, 2004, Problems in exploration seismology and their solutions: Society of Exploration Geophysicists.

Kanasewich, E. R., C. D. Hemmings, and T. Alpaslan, 1973, Nth-root stack nonlinear multichannel filter: GEOPHYSICS, **38**, 327–338.

Khoshnavaz, M. J., K. Chambers, A. Bóna, and M. Urosevic, 2017, Oriented surface passive seismic location using local slopes: GEOPHYSICS, **82**, KS13–KS25.

Lawton, D., M. Bertram, A. Saeedfar, M. Macquet, K. Hall, K. Bertram, K. Innanen, and H. Isaac, 2017, DAS and seismic installations at the CaMI Field Research Station, Newell

County, Alberta: Technical report, CREWES.

Liu, Y., Y. Ma, and Y. Luo, 2020, Source location with cross-coherence migration: GEOPHYSICS, **85**, KS127–KS138.

Lu, W., Z. Yingqiang, and Z. Boran, 2014, Automatic source localization of diffracted seismic noise in shallow water: GEOPHYSICS, **79**, V23–V31.

Macquet, M., D. C. Lawton, A. Saeedfar, and K. G. Osadetz, 2019, A feasibility study for detection thresholds of CO2 at shallow depths at the CaMI Field Research Station, Newell County, Alberta, Canada: Petroleum Geoscience, **25**, 509–518.

Nagano, K., H. Niitsuma, and N. Chubachi, 1989, Automatic algorithm for triaxial hodogram source location in downhole acoustic emission measurement: GEOPHYSICS, **54**, 508–513.

Rost, S., and C. Thomas, 2002, Array seismology: Methods and applications: Reviews of Geophysics, **40**, 2–1–2–27.

Sethian, J. A., and A. M. Popovici, 1999, 3-d traveltime computation using the fast marching method: GEOPHYSICS, **64**, 516–523.

Sheriff, R. E., 2002, Encyclopedic dictionary of applied geophysics, fourth edition: Society of Exploration Geophysicists.

Yew, C. H., and X. Weng, 2015, Mechanics of hydraulic fracturing (second edition), second edition ed.